Comparing variability and trends in observed and modelled global-mean surface temperature

John C. Fyfe,[1] Nathan P. Gillett,[1] and David W.J. Thompson[2]

————

[1]Canadian Centre for Climate Modelling

and Analysis, Environment Canada,

University of Victoria, Victoria, BC,

Canada.

[2]Department of Atmospheric Science,

Colorado State University, Fort Collins, CO,

USA

The observed evolution of the global-mean surface temperature over the twentieth century reflects the combined influences of natural variations and anthropogenic forcing, and it is a primary goal of climate models to represent both. In this study we isolate, compare, and remove the following natural signals in observations and in climate models: dynamically induced atmospheric variability, the El Niño-Southern Oscillation, and explosive volcanic eruptions. We make clear the significant model-to-model variability in estimates of the variance in global-mean temperature associated with these natural signals, especially associated with the El Niño-Southern Oscillation and explosive volcanic eruptions. When these natural signals are removed from time series of global-mean temperature, the statistical uncertainty in linear trends from 1950 to 2000 drops on average by about half. Hence, the results make much clearer than before where some model estimates of global warming significantly deviate from observations and where others do not.

1. Introduction

The twentieth century evolution of global-mean surface temperature reflects the combined influences of naturally occurring climate fluctuations (e.g., oceanic, volcanic, dynamical and possibly solar variability), anthropogenic emissions of various gases and aerosols (e.g., greenhouse gases, sulphate aerosols, and black carbon aerosols), and land use changes (e.g., deforestation). In a recent study some naturally occurring fluctuations were identified and removed by subtracting from the observed record of global-mean surface temperature three known signals of natural climate variability, namely, dynamically induced atmospheric variability associated with anomalous temperature advection over the Northern Hemisphere land masses, the El Niño-Southern Oscillation (ENSO), and explosive volcanic eruptions [Thompson et al. 2009]. The residual time series so obtained reveals near monotonic warming since about 1950, presumably of anthropogenic origin, as well as interannual variations tied to land-sea coupling. Here, we take the logical and important next step of extending this calculation to the multi-model ensemble of twentieth century simulations performed in support of the Intergovernmental Panel on Climate Change (IPCC) Fourth Assessment Report [IPCC, 2007]. The objectives of this study are two-fold: 1) To isolate and compare the observed and simulated signals of natural climate variability. 2) To compare the observed and simulated post-1950 trends in the presence and absence of these naturally occurring climate fluctuations.

2. Data and Models

36   The observed temperature data used in this study are the HadCRUT3 combined land

37   surface temperature and sea surface temperature (SST) datasets [Brohan et al., 2006]. The

38   temperature dataset is available via the Climatic Research Unit at the University of East

39   Anglia and is provided in monthly-mean form on a 5° (latitude) by 5° (longitude) grid, and

40   is expressed as anomalies with respect to the 1961 to 1990 base period. The observed sea-

41   level pressure (SLP) data are provided by the National Center for Atmospheric Research

42   Data Support Section and are also given as monthly-means on a 5° (latitude) by 5°

43   (longitude) grid as described in Trenberth and Paolino (1980). The seasonal cycle is

44   removed from the SLP data by subtracting the long-term mean calculated for the period

45   1950 to 2000 as a function of calendar month.

46   The Atmosphere Ocean Coupled Climate Model (AOGCM) data used in this study are

47   from the Coupled Model Intercomparison Project 3 (CMIP3) [Meehl et al., 2007] database

48   of climate model simulations archived at the Program for Climate Model Diagnostics and

49   Intercomparison (PCMDI) at the Lawrence Livermore National Laboratory. We consider

50   a multi-model ensemble of twentieth century simulations driven with observed greenhouse

51   gas and sulphate aerosol forcing, and in some cases, volcanic forcing. The 24 models con-

52   sidered are BCC-CM1 (A,4), BCCR-BCM2-0 (B,1), CCCMA-CGCM3-1 (C,5), CCCMA-

53   CGCM3-1-T63 (D,1), CNRM-CM3 (E,1), CSIRO-MK3-0 (F,3), CSIRO-MK3-5 (G,1),

54   GFDL-CM2-0 (H,3), GFDL-CM2-1 (I,3), GISS-AOM (J,2), GISS-MODEL-E-H (K,5),

55   GISS-MODEL-E-R (L,2), IAP-FGOALS1-0-G (M,3), INGV-ECHAM4 (N,1), INMCM3-

56   0 (O,1), IPSL-CM4 (P,1), MIROC3-2-MEDRES (Q,3), MIROC3-2-HIRES (R,3), MIUB-

57 ECHO-G (S,5), MPI-ECHAM5 (T,1), MRI-CGCM2-3-2A (U,5), NCAR-CCSM3-0 (V,1),

58 NCAR-PCM1 (W,4) and UKMO-HADCM3 (X,2); with model identifier and number of

59 independent realizations analyzed shown in parentheses. The simulated surface tempera-

60 ture and SLP fields are interpolated onto the same 5° (latitude) by 5° (longitude) grid as

61 the observations and are thereafter treated identically to the observations including mask-

62 ing with observed coverage. All significance testing in this study is at the 95% confidence

63 level.

3. Methodologies

64 The natural climate signals in monthly-mean global-mean surface temperature

65 $T_{GLOBAL}(t)$ are estimated as follows using the method of Thompson et al. [2009].

66 *Dynamically induced signal.* The dynamically induced signal is found on a month-by-

67 month basis by regressing SLP anomaly maps onto normalized land-ocean temperature

68 difference time series for the Northern Hemisphere. The coefficient time series of these

69 SLP regression patterns define the dynamically induced signal $\hat{T}_{DYNAMIC}(t)$.

70 *ENSO signal.* The ENSO signal is estimated using a simple oceanic mixed layer model

71 $C(d/dt)\hat{T}_{ENSO}(t) = F(t) - \hat{T}_{ENSO}(t)/\beta$, where $F(t)$ is an estimate of the anomalous flux of

72 sensible and latent heat in the eastern tropical Pacific; β is a linear damping coefficient set

73 to 2/3 K W^{-1} m^{-2} ; and C is an effective heat capacity of the atmosphere-ocean system

74 per unit area. The heat capacity is obtained such that the correlation coefficient between

75 $\hat{T}_{ENSO}(t)$ and $T_{GLOBAL}(t)$ is maximum based on de-trended data from 1950 through 2000.

76   **The results in this study are largely insensitive to the choice of β, or computed**

77   **values of C.**

78   *Volcanic signal.* The volcanic signal $\hat{T}_{VOLCANO}(t)$ is estimated from the oceanic mixed

79   layer model as above where $F(t)$ is derived from optical thickness data; β is set to 2/3 K

80   $\mathrm{W}^{-1}\,\mathrm{m}^{-2}$; and C is obtained optimally as above. **For the observations we use the Sato**

81   **et al. [1993] optical thickness data. For each model simulation that includes**

82   **volcanic aerosols we use the reconstruction used to force that simulation, i.e.,**

83   **Sato et al. [1993], Amman et al. [2003], or a very similar reconstruction.**

84   **Using $\hat{T}_{DYNAMIC}(t)$, $\hat{T}_{ENSO}(t)$, and $\hat{T}_{VOLCANO}(t)$, a multivariate regression was**

85   **carried out using a prescribed first order autoregressive, AR(1), model for**

86   **the noise $\varepsilon(t)$. (The results are insensitive to higher orders of the AR noise**

87   **model.) In this way we obtain $T_{GLOBAL}(t) = c + \alpha\,t + T_{DYNAMIC}(t) + T_{ENSO}(t) +$**

88   **$T_{VOLCANO}(t) + \varepsilon(t)$ with $T_{DYNAMIC}(t) = \mu\,\hat{T}_{DYNAMIC}$, $T_{ENSO}(t) = \nu\,\hat{T}_{ENSO}$, and**

89   **$T_{VOLCANO}(t) = \xi\,\hat{T}_{VOLCANO}$. The constants α, μ, ν, and ξ are the regression**

90   **parameters and c is a constant.** Finally, we compute $T_{RESIDUAL} = T_{GLOBAL} -$

91   $T_{DYNAMIC} - T_{ENSO} - T_{VOLCANO} = c + \alpha\,t + \varepsilon$ where $T_{RESIDUAL}$ represents the component

92   of T_{GLOBAL} that is linearly unrelated to the natural climate signals. One of the key

93   advantages of this approach **over, say, decadal averaging of the data** is that it

94   removes estimates of these components of natural variability without reducing the time

95   resolution of the data.

4. Results

4.1. Climate evolution and the natural signals

Figure 1 (top panel) shows the evolution of observed and simulated twentieth century global-mean surface temperature anomalies. **As a group the models show good agreement with the observed global-mean warming.** Figure 1 (middle panels) gives the impression that for many models the variance in global-mean temperature associated with the ENSO signal is overestimated, and that there is a significant range of estimates associated with the volcanoes. We will quantify these visual impressions shortly. Figure 1 (bottom panel) shows that with the natural climate signals removed from the observed global-mean temperature time series there is a large discontinuity around 1945, which has been ascribed to uncorrected biases in the SST record [Thompson et al., 2008]. The discontinuity does not appear in the climate model simulations, and hence the mismatch in global-mean surface temperature for the decade around 1945. Because of this discontinuity all subsequent calculations, including the multivariate regressions, are for the period after 1950.

Figure 2 shows the difference in standard deviation between each model and observations for the natural time series (top panels) and residual time series with the linear trend excluded (bottom panel). The bars reflect uncertainties arising from the multivariate regression. Note that the null hypothesis of no significant difference is rejected when the observed and simulated uncertainty ranges taken together exclude zero. The simulated ENSO values show a wide range, with 15 of 24 values deemed inconsistent with observed. Five of the simulated ENSO values are greater than 1.5 times observed, and one is about

116   2.5 times observed. The simulated volcanic values also show a wide range, with 2 of 11

117   values deemed inconsistent with observed, at about 1.5 times observed. The simulated

118   dynamically-induced and de-trended residual times series have 7 and 8 values inconsistent

119   with observed, respectively. In short, the models produce a significant range of estimates

120   of the variance in global-mean surface temperature associated with these climate signals.

4.2. Trends and uncertainties

121   We now turn to an analysis of the trends γ and α in $T_{GLOBAL}(t) = d + \gamma\,t + \eta(t)$ and

122   $T_{RESIDUAL}(t) = c + \alpha\,t + \varepsilon(t)$, respectively, where $\eta(t)$ and $\varepsilon(t)$ are the regression residuals

123   assumed to be AR(1) noise. Figure 3a shows that the observations and models display

124   significant warming trends in both T_{GLOBAL} (red bars) and $T_{RESIDUAL}$ (blue bars). The

125   observed and model-mean trends in T_{GLOBAL} are statistically indistinguishable, with val-

126   ues of about 0.099°C/decade and 0.100°C/decade, respectively. Similarly, in $T_{RESIDUAL}$

127   the observed and simulated trends are about 0.100°C/decade and 0.107°C/decade, respec-

128   tively. However, the variance across the model trends is about 25% smaller in $T_{RESIDUAL}$

129   than in T_{GLOBAL}, indicating a tighter multi-model estimate absent the natural signals.

130   **Figure 3a also shows that of the models with volcanic forcing the majority**

131   **underestimate the observed trend in T_{GLOBAL}, but exhibit $T_{RESIDUAL}$ trends**

132   **much close to that observed.**

133   Figure 3a shows that the individual confidence intervals in the $T_{RESIDUAL}$ are much

134   narrower than in T_{GLOBAL}, especially for the models that include volcanic forcing. It

135   follows that the degree of consistency between a simulated and observed trend could be

136   different depending on whether or not the natural signals are removed. To illustrate this

137   consider the null hypothesis that there is no significant difference between a model and

138   observed trend – which would be rejected if the confidence interval for the difference time

139   series were not overlapping zero. Here the difference time series is the difference between

140   the given model and observed times series. Figure 3b shows that the outcome of the

141   hypothesis test is changed for 7 models going from T_{GLOBAL} to $T_{RESIDUAL}$. For example,

142   the null hypothesis is accepted in T_{GLOBAL} of Models B, G, M, P and W, but rejected in

143   $T_{RESIDUAL}$ because of the drop in uncertainty. On the other hand, the null hypothesis

144   is rejected in T_{GLOBAL} of Models I and O but accepted in $T_{RESIDUAL}$ because of the

145   closer to observed trend estimates. It is also notable that there is no clear relationship

146   between skill in reproducing trends and skill in reproducing natural variance (cf. Figure

147   2). For example, Models I and T have large ENSO biases but near perfect residual trends.

148   This highlights the difficulty in evaluating the ability of climate models to project future

149   climate change based on their ability to simulate past natural variability.

150   To understand the effect of natural signal removal on trend estimates we appeal to

151   Santer et al. [2000; subsection 4.1] who provide trend and uncertainty formulae. To an

152   excellent approximation these formulae recover the trends and uncertainties in Figure 3a

153   (not shown). Uncertainty U involves the variance of regression residuals about the trend

154   line $D^2 = \sum e(t)^2$, as well as effective sample size $n_e \approx n(1 - a_1)/(1 + a_1)$, where n is the

155   number of time samples and a_1 is the lag-1 autocorrelation of $e(t)$. We want to understand

156   how this uncertainty depends partly on the autocorrelation (more autocorrelation means

157   more uncertainty) and partly on the variance around the trend line (more variance means

158   more uncertainty). Accordingly, we use a simple algebraic manipulation of the expressions

in Santer et al. [2000] to obtain $U = A(a_1)D$ where $A(a_1)$ is then, by definition, a monotonically increasing function of a_1. For small differences in trend uncertainty between the global and residual trends we can approximate that difference as arising from parts related to the autocorrelation and the variance: $\Delta U/U \approx \Delta A/A + \Delta D/D$. Figure 4a shows that the observed and model-mean uncertainty is about 50% smaller in $T_{RESIDUAL}$ than in T_{GLOBAL}, due in about equal measure to lower autocorrelation and variance effects in the absence of the natural climate signals.

5. Conclusions

A physically-based approach to isolating the signals associated with dynamically induced atmospheric variability, El Niño-Southern Oscillation (ENSO), and explosive volcanic eruptions has been used in this study to compare and remove the signals of naturally occurring variability in observed and climate model simulated global-mean surface temperature over the twentieth century. We have made clear the significant model-to-model variability in estimates of the variance in global-mean temperature associated with these natural signals, especially with ENSO and explosive volcanic eruptions. We have also shown that the observed and simulated uncertainty in 1950-2000 trends drops by about half when the natural signals are removed, making clearer where the anthropogenic response in some models deviates significantly from observed. The simulated and observed global-mean temperature trends are statistically indistinguishable in 12 of 24 models for the raw data, but in 8 of 24 models for the residual data. Hence, the methodology employed in this study has allowed us to separate the different contributions to variance in global-mean surface temperature, and this has led us to identify some key strengths

and weaknesses in: 1) climate models ability to simulate the observed variance in natural

phenomena and 2) climate models ability to simulate the observed global-warming of the

second half of the 20th century. Interestingly, the results reveal that there is no clear

relationship between a model's ability to simulate the variance of natural phenomena and

the observed global warming.

References

Ammann, C. M., G. A. Meehl, W. M. Washington, and C. S. Zender, 2003: A monthly

and latitudinally varying volcanic forcing dataset in simulations of 20th century climate.

Geophys. Res. Lett., *30*, 1657, doi:10.1029/2003GL016875.

Brohan, P., J.J. Kennedy, I. Harris, S.F.B. Tett, and P.D. Jones (2006), Uncertainty

estimates in regional and global observed temperature changes: A new dataset from

1850. *J. of Geophysical Research*, *111*, D12106, doi:10.1029/2005JD006548.

Intergovernmental Panel on Climate Change (2007), *The Physical Science Basis. Contri-

bution of Working Group I to the Fourth Assessment Report of the Intergovernmental

Panel on Climate Change* [edited by Solomon et al.], Cambridge University Press, Cam-

bridge, United Kingdom and New York, NY, USA, 996 pp.

Meehl, G.A., C. Covey, T. Delworth, M. Latif, B. McAvaney, J.F.B. Mitchell, R.J. Stouf-
    fer, and K.E. Taylor (2007), The WCRP CMIP3 multi-model dataset: a new era in
    climate change research. *Bulletin of the American Meteorological Society, 88(9)*, 1383-
    1394.

Santer et al. (2000), Statistical significance of trends and trend differences in layer-average
    atmospheric temperature rise, *J. of Geophysical Res., 105(D6)*, 7337-7356.

Sato, M.J., J.. Hansen, M.P. McCormick, and J.B. Pollack (1993), Stratospheric aerosol
    optical depth, 1850-1990, *J. of Geophysical Res., 98(D12)*, 22,987-22,994.

Thompson,D.W.J., J.J. Kennedy, J.M. Wallace, and P.D. Jones (2008), A large discontinu-
    ity in the mid-twentieth century in observed global-mean surface temperature. *Nature*,

Thompson, W.J., J.M. Wallace, P.D. Jones, and J.J. Kennedy (2009), Identifying signa-
    tures of natural climate variability in time series of global-mean surface temperature:
    Methodology and insights. *J. of Climate*, 22, 6120-6141.

Trenberth, K.E., and D.A. Paolino (1980), The Northern Hemisphere sea level pressure
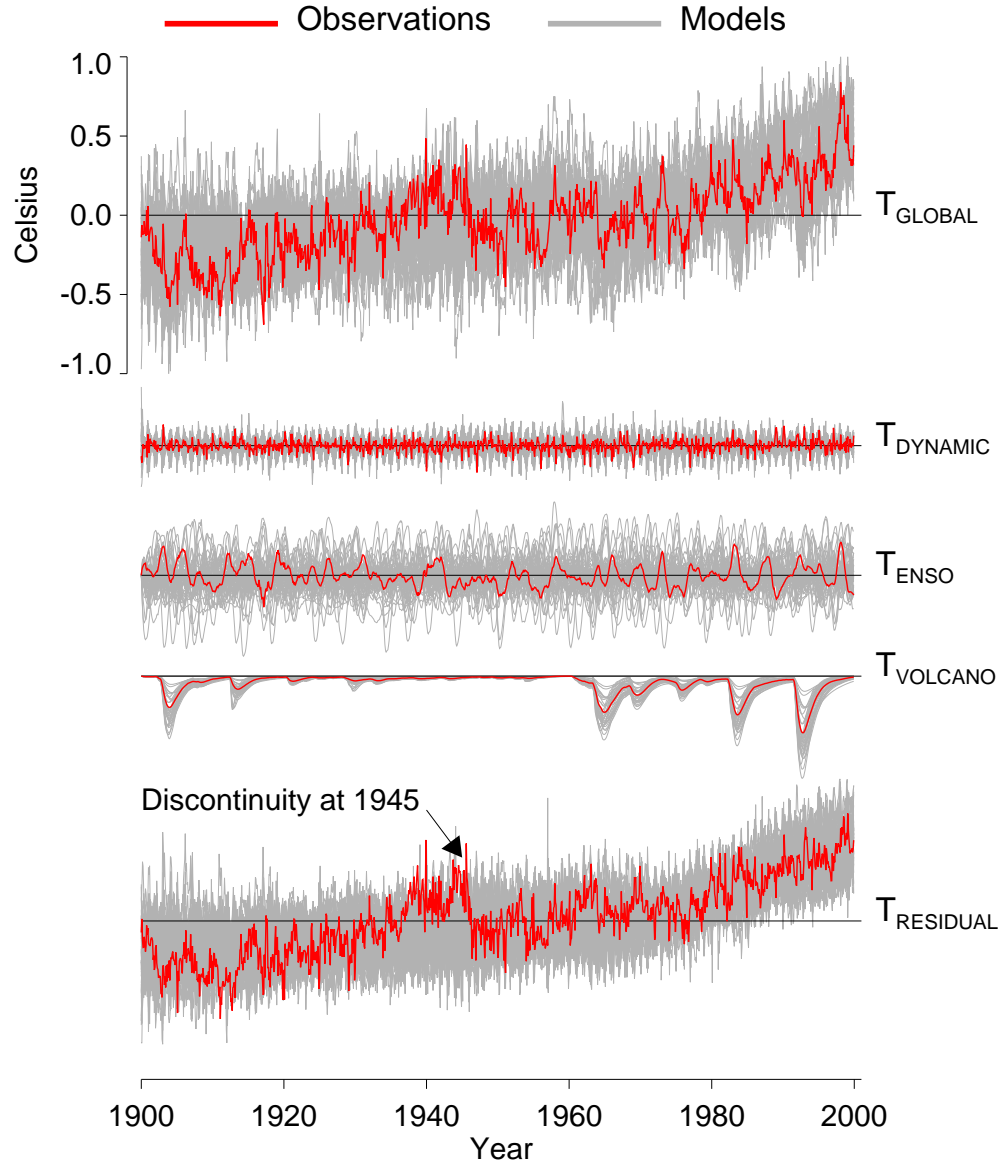   data set: Trends, errors and discontinuities. *Mon. Wea. Rev., 108*, 855-872.

Figure 1. The monthly-mean global-mean surface temperature anomalies; (middle) the natural signals; (bottom) the residual time series found by removing the natural signals from T_{GLOBAL}.
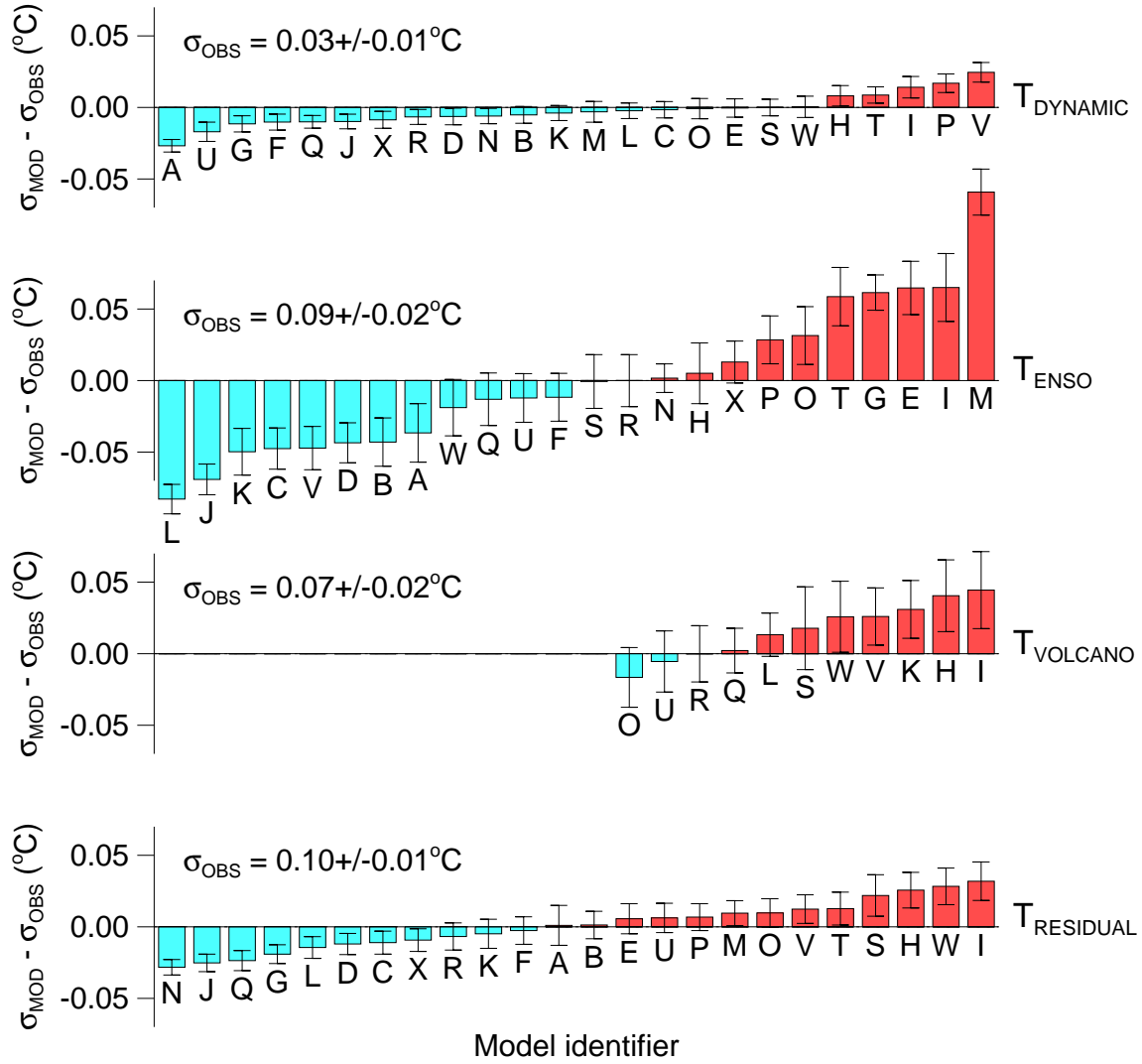
Figure 2. The difference in the standard deviation of temperature between each model and the observations. For the models the standard deviation and uncertainty is the average over all available realizations.
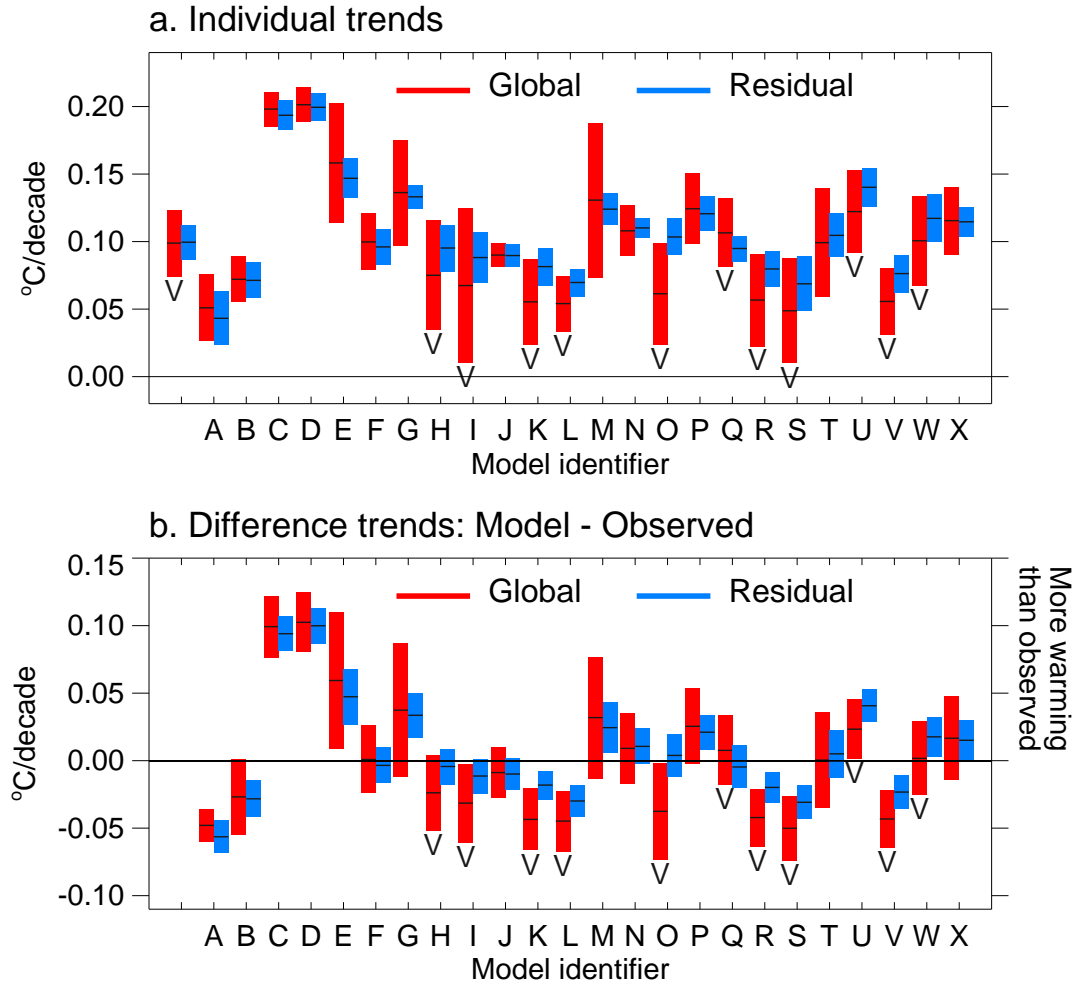
Figure 3. a. Individual trends. For the models both the mean and uncertainties are realization-means. b. Difference trends based on the difference between the model and observed time series. A bar not overlapping zero indicates a rejected null hypothesis that there is no significant difference between the given model trend and the observed trend. "V" denotes the presence of volcanic forcing.
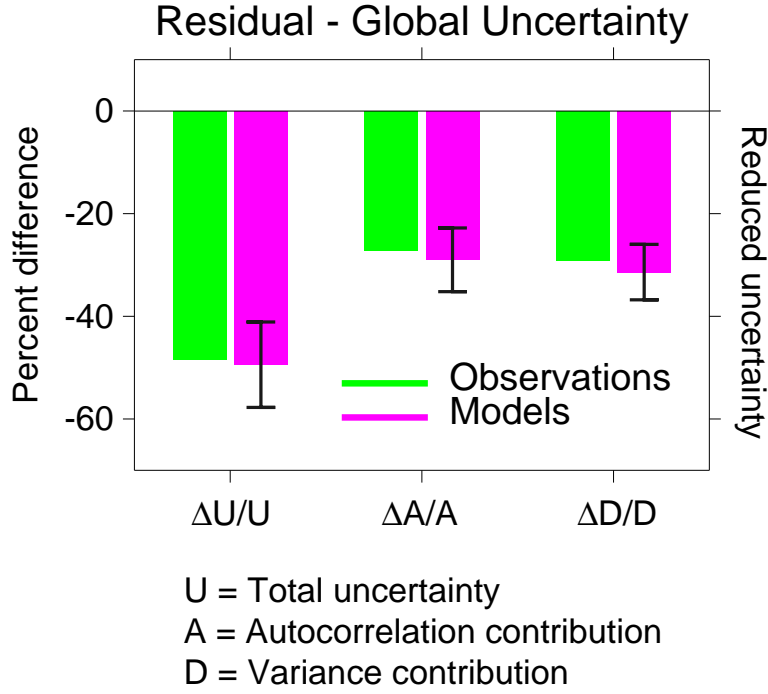
Figure 4. Percent difference in the trend uncertainty U (as in Figure 3a) between $T_{RESIDUAL}$ and T_{GLOBAL}. As described in Section 4 the trend uncertainty U is such that $\Delta U/U \sim \Delta A/A +$ $\Delta D/D$, where $\Delta A/A$ and $\Delta D/D$ measure contributions arising from differing autocorrelation and differing variance, respectively. Error bars are multi-model confidence intervals.